RSC Advances

PAPER

View Article Online
View Journal | View Issue

Cite this: *RSC Adv.*, 2025, **15**, 17080

Low-temperature, *in situ* growth of graphene *via* the active hexatomic aromatic ring species of dissociated α-naphthol

Caijiao Tian,[ab] Yi Zhang,*[a] Meng Zhou,*[a] Shiding Zhang,[b] Baohong Tian,[a] Chunhe Chu[a] and Ke Jing[a]

Received 10th March 2025
Accepted 21st April 2025

DOI: 10.1039/d5ra01718a

rsc.li/rsc-advances

Using small-molecule carbon sources such as α-naphthol, graphene (Gr) can be generated at relatively low temperatures (600 °C). By optimizing factors such as raw materials, carbon source concentration, growth temperature, and time, the few layers and high-quality Gr on copper (Cu) substrates is achieved, and the properties of Gr are analyzed. Pretreatment of the Cu substrates can enhance the smoothness and flatness of the Cu surface, thereby promoting uniform adsorption of carbon sources and continuous growth of a Gr layer. As the concentration of carbon sources or the growth temperature increases, although the decomposition rate of the carbon source accelerates and ensures adequate carbon supply, the formation of more defects can occur. A deep analysis is provided on the nucleation and growth processes of Gr prepared using the α-naphthol precursor, unveiling the dissociation pathway of α-naphthol and the roles of intermediate active aromatic species with two hexatomic rings in nucleating and assembling the Gr lattice.

1 Introduction

Graphene (Gr) has stimulated numerous studies for more than half a century owing to its potential in applications such as in high-speed transistors, phonon detectors, transparent electrodes, and sensors.[1–4] Establishing synthetic routes to obtain high-quality Gr films has attracted considerable research interest. Current methods for the synthesis of Gr mainly include mechanical exfoliation of graphite,[5] reduction of Gr derivatives such as Gr oxide,[6] and hydrocarbon source chemical vapor deposition (CVD) using transition metal catalysts.[7–9] However, CVD using methane as a typical carbon source is complex, and the *in situ* growth temperature is usually around 1000 °C. Because CVD growth at high temperatures is undesirable for many practical reasons, including high energy consumption, potential safety hazards, and increased complexity in process control, significant efforts have been made to lower the growth temperature of high-quality Gr films using alternative carbon precursors. Carbon can be deposited in the form of Gr directly on metal by annealing carbon precursor materials.[10–12] Copper (Cu) is widely used as a growth substrate owing to its low cost and good catalytic effect. Zhang *et al.*[13] utilized sucrose as a carbon source to grow Gr on a Cu substrate through annealing at 800 °C. The I_D/I_G ratio of Gr/Cu composite powders is about 0.53, with an ultralow loading content of Gr of 0.096 wt%. Considering the complex pyrolysis reactions occurring during the decomposition of sucrose, carbon deposition on a Cu substrate may be uneven, thereby disrupting the continuity and uniform thickness of the Gr layer. PMMA[14,15] is also frequently used as a carbon source for the *in situ* growth of Gr. However, PMMA is a macromolecular polymer with a complex molecular structure, and Gr synthesis requires a complicated chemical reaction process[16] and a high growth temperature of 800 °C. In addition, carbon clusters in the earlier nucleation stage take linear forms rather than cyclization structures, and the subsequent process of *in situ* growth of Gr from methane, sucrose, or PMMA involves rearrangement and assembly of carbon atoms into hexatomic rings. More strikingly, it has been demonstrated that the growth temperature can be significantly reduced when different aromatic carbon sources are used for the *in situ* growth of Gr on Cu.[17–19]

In this study, α-naphthol, with two hexatomic rings, was chosen as an aromatic carbon source. The morphology and characteristics of Gr grown on Cu at different temperatures and times are analyzed with an explanation provided for its nucleation and growth mechanisms. By optimizing factors such as raw materials, temperature, time, and carbon source concentration, it is possible to successfully grow Gr materials with excellent properties on a Cu substrate, providing new insights for the development of low-cost and efficient Gr synthesis methods.

[a]*Henan University of Science and Technology, School of Materials Science and Engineering, 263, Kaiyuan Avenue, Luoyang, China. E-mail: yizhang@haust.edu.cn; zhoumeng0902@126.com*

[b]*Anyang Institute of Technology, School of Materials Science and Engineering, Huanghe Avenue, Anyang, China*

2 Materials

2.1 Material preparation

Cu flakes (99.9 wt% purity; a diameter of about 20 μm; purchased from Shanghai Mao Guo Nanotechnology Co., Ltd) were chosen as original materials because their large surface area enables the adsorption of sufficient carbon precursors on the surface. α-Naphthol ($C_{10}H_8O$; Sinopharm Chemical Reagent Co., Ltd) was used as the carbon precursor. Cu flakes were annealed under an H_2/Ar atmosphere at 350 °C for 2 h to remove oxides and other impurities to obtain the desired powders. α-Naphthol ($C_{10}H_8O$) was dissolved in ethanol solution (300 mL) and stirred for a period of time to obtain a uniform and transparent solution. Subsequently, 30 g Cu powder was added to this solution. The composite powders prepared with Cu to α-naphthol mass ratios of 10 : 0.1, 10 : 0.3, and 10 : 0.5 were designated as Gr/Cu-0.1, Gr/Cu-0.3 and Gr/Cu-0.5, respectively. The mixture was then heated at 75 °C under constant magnetic stirring until the solution vaporized completely. After drying at 80 °C for 4 h to remove the solvent, the α-naphthol/Cu composite powders were transferred to a quartz tube, followed by *in situ* Gr growth under 20% H_2/Ar atmosphere. The Gr/Cu composite powders were obtained *via* fast-cooling to room temperature under an H_2/Ar atmosphere. Gr was obtained from the Gr/Cu composite powders by etching the Cu matrix using $FeCl_3$/HCl solution. Fig. 1 illustrates the *in situ* Gr growth processes.

2.2 Microstructure of Gr/Cu mixed-powders and Gr

The morphologies of the original Cu, α-naphthol/Cu, and Gr/Cu composite powders were observed using scanning electron microscopy (SEM) (JSM-IT800). The morphologies and microstructures of the as-grown Gr were observed *via* transmission electron microscopy (TEM) (JEM-2100F) and high-resolution transmission electron microscopy (HRTEM) (JEM-2100F). Raman spectroscopy (Renishaw, inVia microscope) was performed with a 532 nm laser to measure the defects in the Gr grown from α-naphthol. The carbon content in the composite powders was analyzed through a C/S analyzer (LECO/CS230). X-ray diffraction (XRD) was performed using a Panalytical X'Pert X-ray diffractometer.

3 Results and discussion

3.1 The influence of Cu matrix annealing on the *in situ* growth of Gr

Since Gr is grown *in situ* during the heat treatment process, factors including Cu substrates, carbon precursor content, growth temperature and time may influence the quality of Gr.[16,20] A detailed discussion on these aspects is given below.

The surface smoothness and crystal grain orientation of the Cu substrate play important roles in the *in situ* growth of Gr. The morphology of the original flaky Cu powders is presented in Fig. 2a, which shows that the diameter of Cu powders is about 20 μm and the thickness is about 1 μm. The flake-like Cu powders with a large specific surface area provide a larger area for the adherence of carbon sources. Fig. 2b shows the XRD image of Cu powders before and after annealing. All types of Cu powders exhibited diffraction peaks around 43°, 50°, and 74°, corresponding to the (111), (200), and (220) crystal planes of pure Cu, respectively. The $I_{(111)}/\sum I_{(all)}$ of the Cu powders was 0.53 and 0.60 before and after annealing, respectively. The images show that after annealing at 350 °C for 2 hours in 5% H_2/Ar atmosphere, the Cu powders exhibited a higher (111) orientation. During annealing in a hydrogen atmosphere, grains may undergo recrystallization and grain growth, tending to evolve toward a low-energy state and transform the crystal orientation towards (111). The diffusion rate of carbon atoms, the adsorption rate, and the nucleation rate of Gr could vary significantly from different crystal planes of the Cu substrate. Cu(111) (with an atomic spacing of 2.56 Å) has high structural consistency with the two-dimensional Gr (0001) (with an atomic spacing of 2.46 Å). This results in a large coverage area and a fast nucleation rate of Gr grown on the Cu surface.[14,15,21,22]

In addition, the XRD image shown in Fig. 2b reveals that the unannealed Cu powders exhibit a diffraction peak around 36.5°, corresponding to the (111) crystal planes of Cu_2O. After annealing, this diffraction peak disappears. Thus, annealing of the Cu powders under 5% H_2/Ar atmosphere can effectively remove Cu oxide particles, resulting in impurity-free surfaces. This facilitates the uniform adsorption of α-naphthol onto the Cu surface. Fig. 2c shows that α-naphthol distribution on the surface of the Cu powder without annealing is uneven. The *in situ* growth of Gr on the surface of Cu without annealing, shown in Fig. 2e, results in obvious agglomeration. Fig. 2d and f reveal

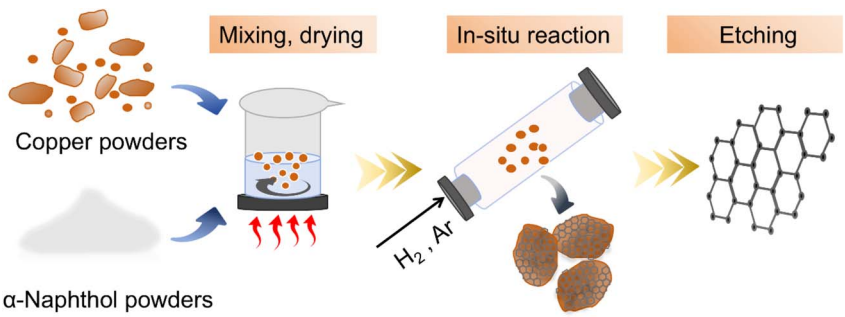

Fig. 1 Schematic of *in situ* Gr growth processes.

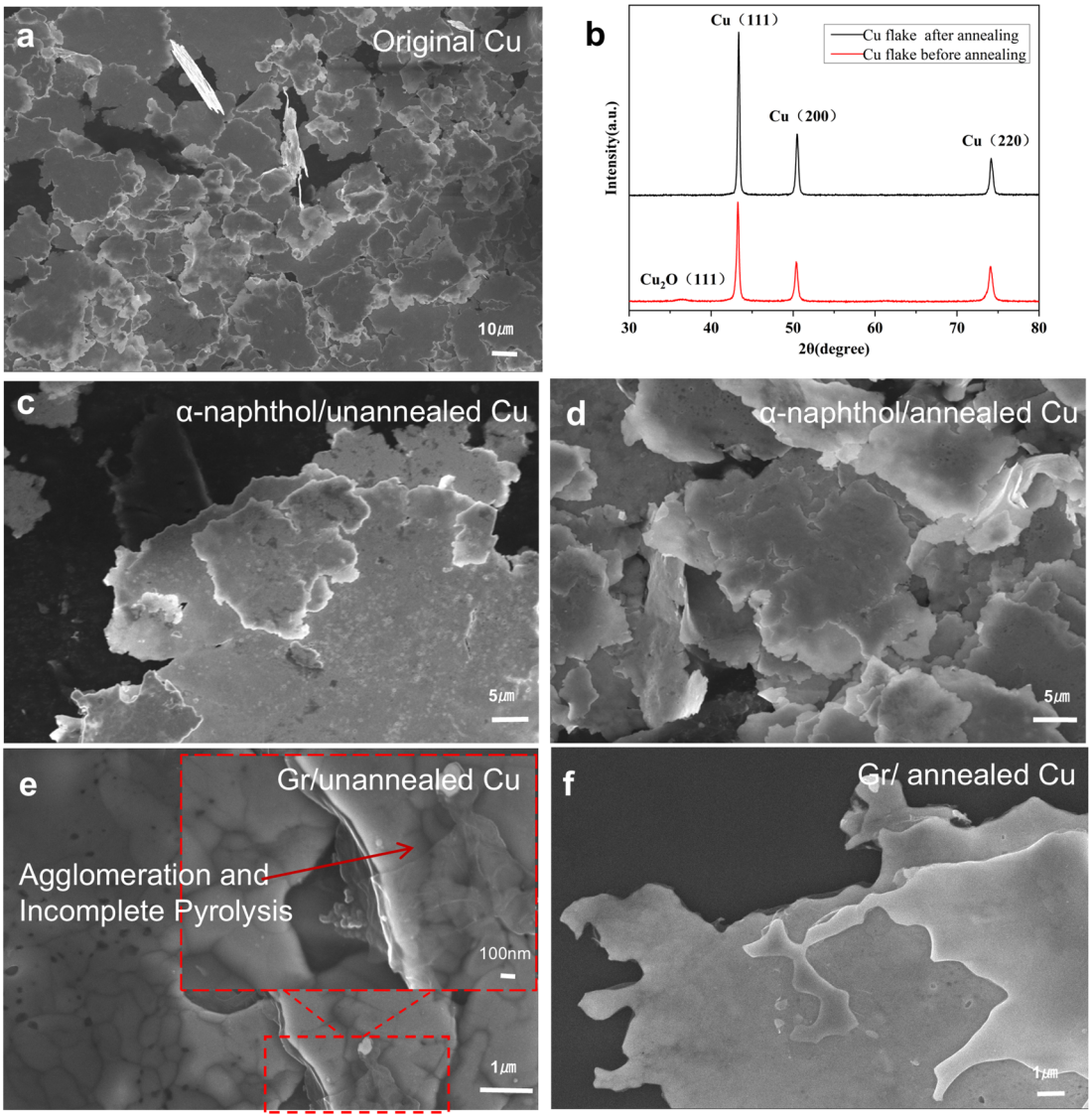

Fig. 2 (a) SEM image of the original Cu powders. (b) XRD patterns of Cu powders before and after annealing. (c) α-Naphthol/unannealed Cu. (d) α-Naphthol/unannealed Cu. (e) Gr/annealed Cu. (f) Gr/annealed Cu.

that the annealed Cu can evenly adsorb α-naphthol on its surface, and the *in situ* growth of Gr on the Cu surface occurs without significant agglomeration. Compared with unannealed Cu, Cu powders annealed at 350 °C for 2 h under 5% H_2/Ar atmosphere are beneficial to grow high-quality Gr because the removal of Cu oxide particles improves the catalytic activity.

3.2 The influence of α-naphthol content on *in situ* Gr growth

The SEM morphologies of the Gr/Cu composite powders obtained using three different carbon source concentrations at 700 °C for 20 min are shown in Fig. 3a–c. The products on the surface of the Cu powders exhibit the typical translucent layered structure of Gr, indicating that the Cu powders possess the catalytic activity to transform nearby α-naphthol into Gr during high-temperature treatment. In the Gr/Cu composite powders, the Cu substrate can be clearly seen beneath the Gr, indicating the high light transmission and good crystallinity of *in situ* grown Gr. The morphology of the Gr/Cu-0.5 (Fig. 3c) composite powders is significantly different from that of Gr/Cu-0.1 (Fig. 3a) and Gr/Cu-0.3 (Fig. 3b). For Gr/Cu-0.1 and Gr/Cu-0.3, the presence of thin wrinkles indicates the growth of a few layers of Gr on the Cu substrate. Super-saturation of the precursor for Gr/Cu-0.5, should lead to considerably faster Gr growth, and the grown Gr may be more wrinkled and thicker owing to the increase in the precursor content. This was further analyzed using Raman spectroscopy and TEM.

The structural defects in the as-grown Gr in the three composite powders were further evaluated through Raman spectroscopy, which is widely acknowledged as a characterization technique employed for the assessment of the structural integrity of Gr; the results are displayed in Fig. 3d–f. The G band, a radial C–C stretching mode of sp^2 hybridized carbon, and the D band, originating from a first-order zone boundary

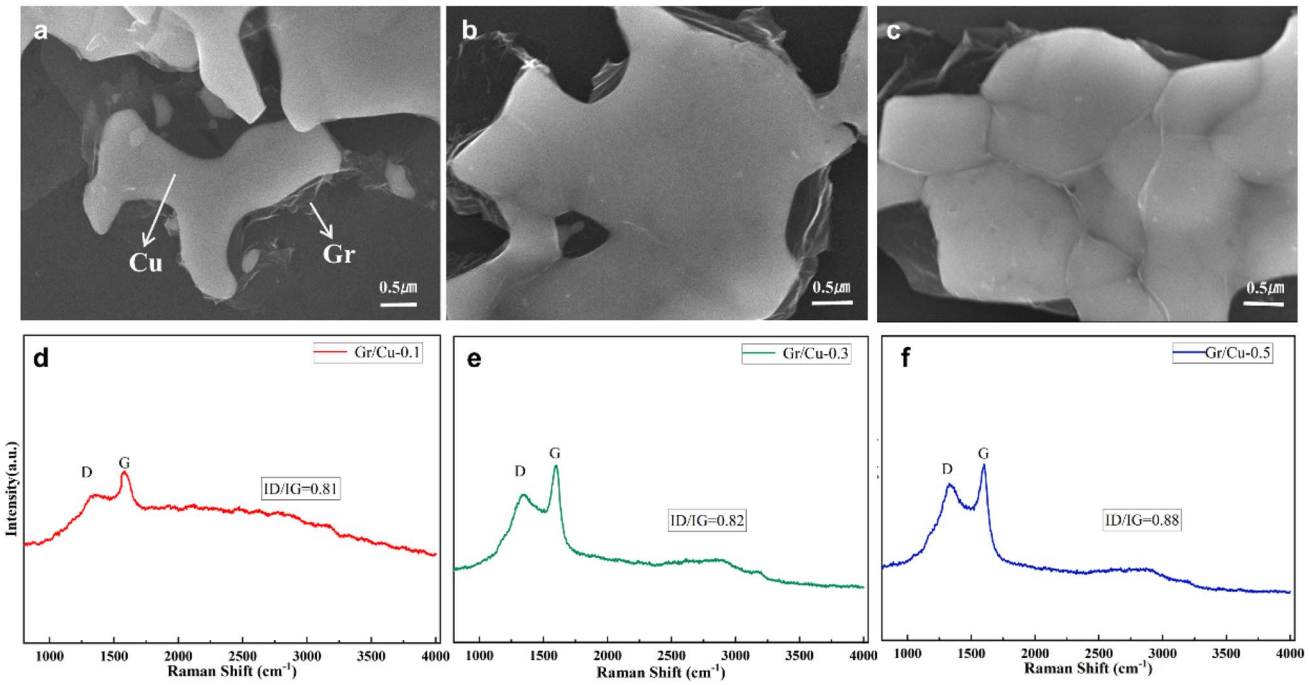

Fig. 3 SEM morphologies of (a) Gr/Cu-0.1, (b) Gr/Cu-0.3, and (c) Gr/Cu-0.5 powders. Raman spectra of (d) Gr/Cu-0.1, (e) Gr/Cu-0.3, and (f) Gr/Cu-0.5 powders.

phonon mode associated with defects, appear at ≈1580 cm^{-1} and ≈1350 cm^{-1}, respectively.[23–25] Usually, a higher intensity ratio value of the D to G peaks (I_D/I_G) may indicate lower Gr crystallinity and higher defect density.[14,21] As shown in Fig. 3d, the I_D/I_G ratios of Gr/Cu-0.1 and Gr/Cu-0.3 are about 0.81. The ratio is larger than that of Gr synthesized *via* chemical vapor deposition (CVD) using methane[26,27] as the carbon source, but similar to, or even lower than that of Gr grown *in situ via* thermal pyrolysis from organic compounds and chemical reduction of graphene oxide (GO) obtained from oxidation and delamination of graphite. For example, the ratio is 0.899 using sucrose,[28] 0.79 using liquid paraffin[20] and 0.89 using PMMA[29] as the carbon source; the ratio is 1.13 for 0.1 wt% rGO/Cu composites.[30] The results indicate good crystallinity and structural integrity of the Gr obtained from organic compounds through *in situ* growth *via* thermal pyrolysis. With an increasing carbon precursor content, the I_D/I_G ratio of Gr/Cu-0.5 increases to 0.87, revealing an increase in the defects in Gr. This may be due to the increased numbers of folds and layers and agglomeration of Gr or incomplete conversion of solid carbon sources. The ratio may ultimately affect the properties and performance of the Gr. The nucleation and growth of Gr requires a suitable amount of carbon source. When sufficient active carbon atoms are assembled on Cu particle surfaces, nucleation and growth of Gr take place. A low content of carbon may enable Gr to form crystalline layers and prevent the growth of thick and agglomerated structures. Increasing the amounts of solid carbon sources may break down and agglomerate excess carbon. The growth of Gr may then be thicker, and the Gr may even agglomerate to form carbon-rich areas, which may lead to more defects in the Gr.

To further explore the microstructures and characteristics of the *in situ* grown Gr in composite powders with different contents, after corroding the Cu matrix with $FeCl_3$/HCl solution, the Gr was observed *via* TEM and HRTEM. In Fig. 4a and b, the typical wrinkled structural features of Gr can be seen clearly, with the high transparency resulting from the ultrathin thickness and flexibility of the Gr. According to the HRTEM image of the edge area in Fig. 4b, the thickness of Gr is equivalent to 1–3 layers, resulting in an ultralow Gr loading content of 0.096 wt% in the Gr/Cu-0.1 composite powders based on C–S analysis. For Gr/Cu-0.3 (Fig. 4c and d), the thickness is equivalent to 4–6 layers, with a Gr loading content of 0.26 wt%. However, for Gr/Cu-0.5 (Fig. 4e and f), the thickness is about 3 nm and is composed of more than 10 layers. The areas with higher contrast may be residual Cu particles. Since Gr has strong chemical resistance to corroding solution, Cu covered with multiple layers of Gr could not be completely corroded easily,[31] and some residual nano-Cu particles can be seen in the TEM images. TEM and HRTEM images show that the number of Gr layers increased with the concentration of carbon sources, which is consistent with the SEM analysis and Raman results.

3.3 The influence of growth temperature and time on the *in situ* growth of Gr

In addition to raw materials, growth temperature is a crucial factor that directly affects the catalytic activity of Cu powders and the activity of carbon atoms and their groups. It further affects the nucleation and growth of Gr *in situ*. To further explore the growth behavior and identify suitable growth conditions for α-naphthol-based *in situ* growth of Gr, a series of

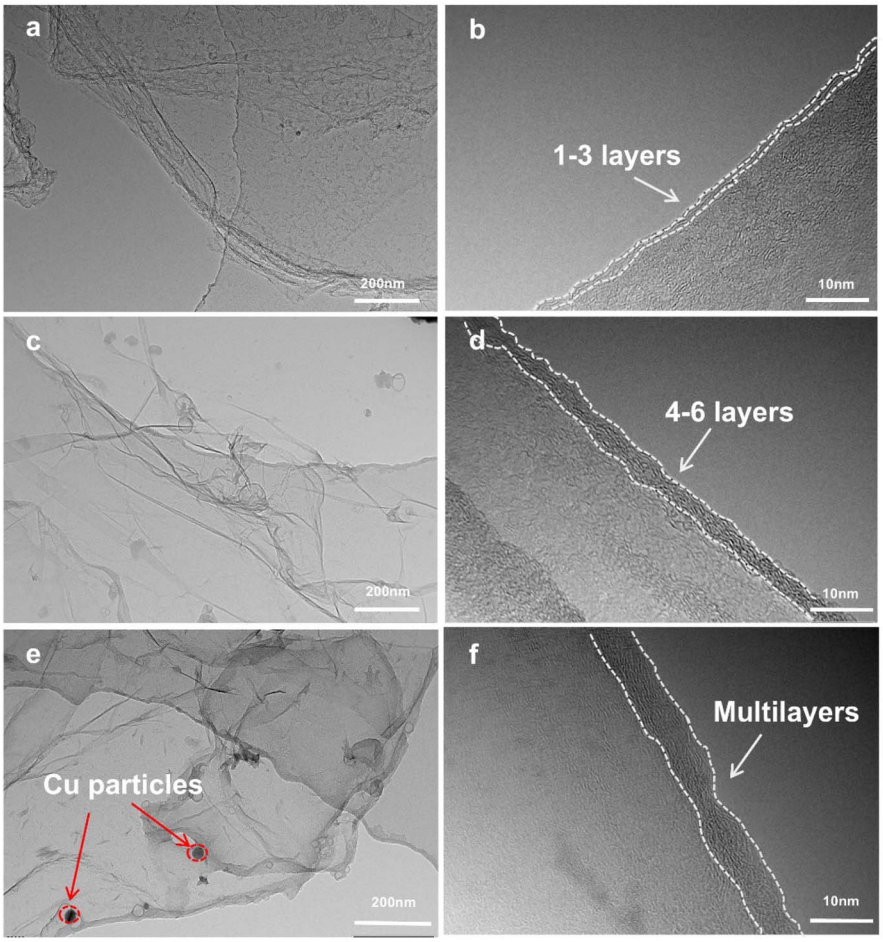

Fig. 4 TEM and HRTEM images of the Gr after corroding Cu from (a and b) Gr/Cu-0.1, (c and d) Gr/Cu-0.3 and (e and f) Gr/Cu-0.5 powders.

experiments were conducted with various growth temperatures and times. Fig. 5 shows the microstructures and Raman spectra of Gr/Cu composite powders grown at 600 °C, 700 °C, and 800 °C for 20 min. Fig. 5a shows that Gr can be grown at a temperature as low as 600 °C, indicating that the small-molecule carbon source α-naphthol can generate high-quality Gr ($I_D/I_G \approx 0.92$) at relatively low temperatures. With an increase in growth temperature, the light transmission and crystallinity of Gr change. As shown in Fig. 5b and Fig. 5e, typical folds of the Gr films, with high transparency and a smooth surface, are formed at 700 °C and 800 °C, with higher quality (Fig. 5g). The higher temperature increases the rate of carbon source cracking and ensures the supply of carbon atoms. The Gr folds become more numerous and thicker when the temperature reaches 800 °C, as shown in Fig. 5f, and the defects increase accordingly. The multilayer growth of Gr is likely due to a higher α-naphthol decomposition rate and higher carbon solubility at the higher temperature, making more carbon species available in the Cu substrate for precipitation upon cooling.

In addition, growth time affects the morphology and the number of defects in Gr. Raman results (Fig. 6a) indicated that the structural disorder of carbon species decreased at 600 °C with increasing reaction time. This is strong evidence that structural healing occurs during the formation of Gr. Not coincidentally, the Raman analysis result also demonstrates similar structural healing at 700 °C and 800 °C for 10 min and 20 min (Fig. 6b and c). However, as the reaction time increases at high temperatures, there is a noticeable aggregation of Gr and the number of defects increases. The combination of appropriate temperature and time facilitates the formation of Gr with high crystallinity and high quality. Since high-quality Gr can be grown at 700 °C for 20 min, it can be deduced that a better catalytic effect can be achieved at this temperature.

3.4 Growth mechanism

The α-naphthol based growth of Gr on the Cu powders could be divided into multiple processes: (I) α-naphthol molecules are adsorbed on the Cu surface and dissociate into active aromatic species with two hexatomic rings following the pathway of dehydroxylation and dehydrogenation, (II) active aromatic species aggregate to nucleate on the active sites of the Cu substrate, and (III) the growth of Gr proceeds by attaching active carbon species to the edges, as illustrated in Fig. 7. In the initial process, α-naphthol dissociates into aromatic species *via* dehydroxylation and dehydrogenation owing to the high temperature. For the dissociation of $C_{10}H_7OH$, several main

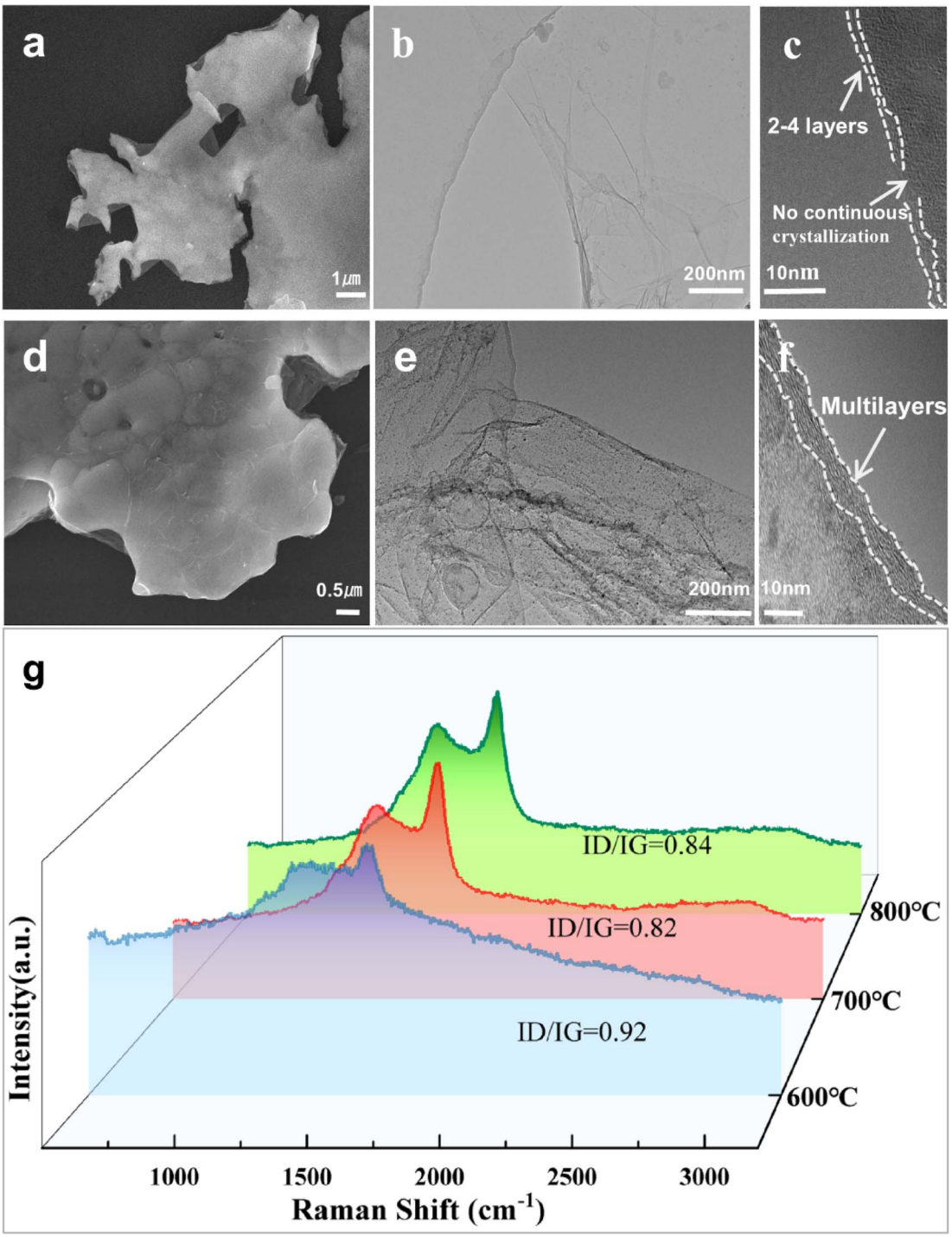

Fig. 5 SEM morphologies of Gr/Cu powders pyrolyzed at (a) 600 °C and (d) 800 °C for 20 min. TEM and HRTEM images of Gr after corroding Cu from (b and c) 600 °C for 20 min and (e and f) 800 °C for 20 min. (g) Raman spectra of Gr/Cu powders.

possible pathways are predicted: $C_{10}H_7OH \rightarrow C_{10}H_6OH + H \rightarrow C_{10} + OH$, $C_{10}H_7OH \rightarrow C_{10}H_7 + OH \rightarrow C_{10} + H$ and $C_{10}H_7OH \rightarrow 10C + 7H + OH$. One of the dominant pathways of α-naphthol dissociation can be expressed as $C_{10}H_7OH \rightarrow C_{10}H_7 \rightarrow C_{10}$. The reaction may produce several by-products in addition to the main product, such as hydrocarbons and carbon oxides. C atoms may also emerge on the Cu surface because the dissociation of the C–C bond is not forbidden during the high-temperature growth process. The introduced hydrogen dissociates on the Cu substrate to form active hydrogen atoms, which could facilitate the catalytic pyrolysis of α-naphthol.

During the growth of Gr, the sufficient carbon sources assembled on Cu particle surfaces can continue to decompose into active aromatic species at high temperatures. The active

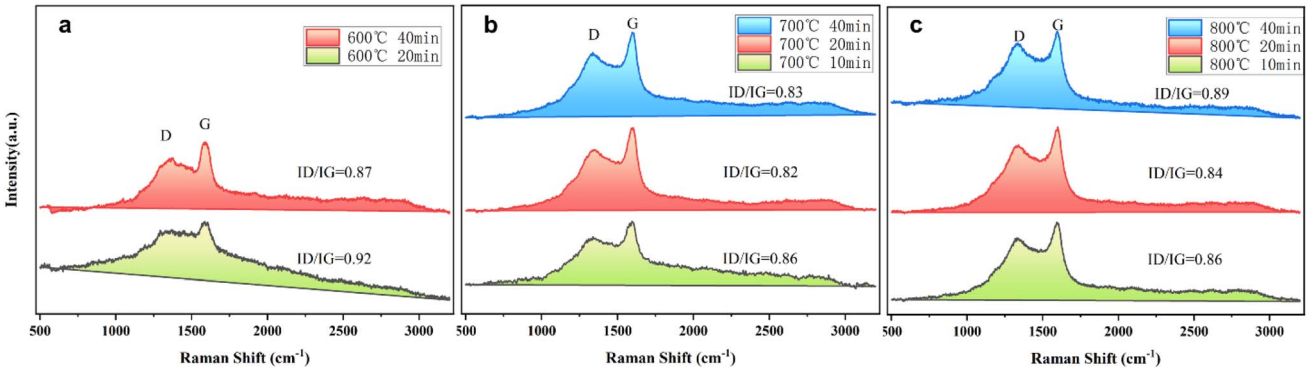

Fig. 6 Raman spectra of Gr/Cu powders obtained from α-naphthol pyrolysis at (a) 600 °C, (b) 700 °C, and (c) 800 °C for different times.

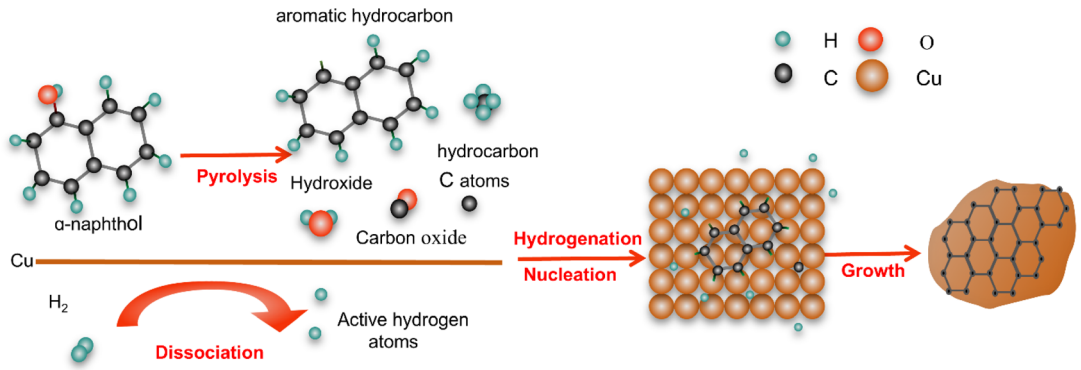

Fig. 7 A schematic to illustrate the processes involved in α-naphthol based *in situ* growth of Gr on the Cu substrate.

aromatic species can either form a new nucleation center at a defect site on the Cu substrate or attach to an existing Gr nucleus to facilitate its continuous growth. Adjacent Gr regions can then connect to each other, forming a continuous Gr film on the Cu substrates.[29,31] The above characterization and analysis suggest a novel model for the nucleation and growth mode of multi-layered Gr. As illustrated in Fig. 8: (a) Frank–van der Merwe growth occurs when the adhesive forces between the growing material and the substrate are much stronger than the cohesive forces between the growing material particles. (b) Volmer–Weber growth is opposite to Frank–van der Merwe growth, where the cohesive forces between the growing material

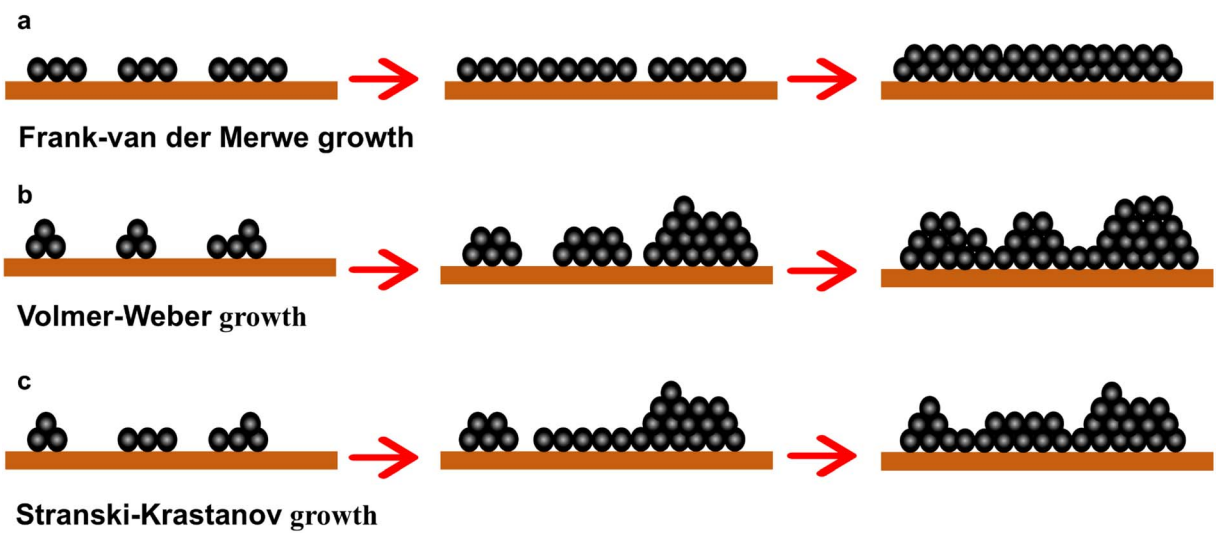

Fig. 8 Three basic modes of nucleation during the initial stage, and growth of the thin film. (a) Frank–van der Merwe growth, (b) Volmer–Weber growth, (c) Stranski–Krastanov growth.

particles are greater than the adhesive forces between the material and the substrate. (c) Stranski–Krastanov growth is an intermediate growth mode between Volmer–Weber growth and Frank–van der Merwe growth.[32]

Clear layer islands appeared in Gr/Cu-0.5 (Fig. 3c) and Gr/Cu grown at 800 °C for 20 min (Fig. 5d). It can be concluded that when the content of carbon sources or growth temperature increase, the growth mode changes from Frank–van der Merwe to Stranski–Krastanov growth. Physical or chemical inhomogeneities of the underlying Gr, such as boundaries and impurities, could serve as nucleation sites for the epitaxy of additional layers. After nucleation, the growth process continues with a high anisotropic nature. Compared with the inert surface of Gr nuclei bonded by weak interlayer van der Waals interactions, edges with dangling bonds are much more active in binding covalently with incoming atoms or fragments. Consequently, the lateral growth rate can be much faster than the vertical growth rate.[33] With an increase in carbon source concentration, the Gr becomes thicker and even agglomerates. The strain energy increases with Gr thickness because of the lattice constant mismatch between the Gr and Cu substrate. To relax this part of the energy, when Gr grows to a certain thickness, the growth mode changes from Frank–van der Merwe to Stranski–Krastanov growth (as shown in Fig. 3c). Similarly, as the growth temperature rises (Fig. 5d), the growth mode changes because the thickness of the Gr layer increases owing to a higher α-naphthol decomposition rate and more carbon available. The lower growth temperature could also decrease the accumulation of strain energy during the cooling process and reduce the mismatch of the surface area between the Gr and the Cu substrate.[34]

4 Conclusions

(1) Gr can be grown *in situ* at a temperature as low as 600 °C, indicating that the small-molecule carbon source α-naphthol can generate a few layers of high-quality Gr at low temperatures. Higher quality Gr can be grown at 700 °C for 20 min.

(2) The Cu matrix is annealed at 350 °C for 2 h under 5% H_2/Ar atmosphere to obtain impurity-free surfaces and a higher ratio of (111) orientation. α-Naphthol density (0.1 wt%) as well as the growth temperature and time (700 °C for 20 min) affect the quality of Gr, enabling Gr to grow in-plane and splice together to generate Gr with fewer defects and fewer layers.

(3) α-Naphthol molecules dissociate into active aromatic species following the pathway of dihydroxylation and dehydrogenation. The active aromatic species aggregate to nucleate Gr on the active sites of the Cu substrate. As the thickness of Gr increases, the growth mode changes from Frank–van der Merwe to Stranski–Krastanov growth.

Data availability

The data that support the findings of this work are available from the corresponding author [Y. Zhang] upon reasonable request.

Author contributions

Caijiao Tian: conceptualization, methodology, investigation, data analysis, writing – original draft, and writing – review and editing. Yi Zhang: supervision, validation, and funding acquisition. Meng Zhou and Yi Zhang contributed equally to this work. Chunke Chu, Ke Jing, and Baohong Tian: investigation and data analysis.

Conflicts of interest

There are no conflicts to declare.

Acknowledgements

This work was supported by the National Natural Science Foundation of China (52071134, 52374367), the Program for Innovative Research Team at the University of the Henan Province (22IRTSTHN001), Leading Talents of Science and Technology in the Central Plain of China (244200510029), the Joint Foundation for Science and Technology Research and Development Plan of Henan Province (232103810030, 232103810031), Key Research and Development Program of Henan Province (231111232000, 231111231300).

Notes and references

1 N. Tajima, T. Kaneko, J. Nara and T. Ohno, *Surf. Sci.*, 2016, **653**, 123–129.
2 S. Lu, C. Tian, X. Wang, L. Zhang, K. Du, K. Ma and T. Xu, *Compos. Sci. Technol.*, 2018, **158**, 94–100.
3 A. Montanaro, W. Wei, D. De Fazio, U. Sassi, G. Soavi, P. Aversa, A. C. Ferrari, H. Happy, P. Legagneux and E. Pallecchi, *Nat. Commun.*, 2021, **12**, 2728.
4 J.-Y. Hong, W. Kim, D. Choi, J. Kong and H. S. Park, *ACS Nano*, 2016, **10**, 9446–9455.
5 K. S. Novoselov, D. Jiang, F. Schedin, T. J. Booth, V. V. Khotkevich, S. V. Morozov and A. K. Geim, *Proc. Natl. Acad. Sci. U. S. A.*, 2005, **102**(30), 10451–10453.
6 S. Stankovich, R. D. Piner, S. T. Nguyen and R. S. Ruoff, *Carbon*, 2006, **44**, 3342–3347.
7 M. Regmi, M. F. Chisholm and G. Eres, *Carbon*, 2012, **50**, 134–141.
8 W. Fang, A. L. Hsu, Y. Song, A. G. Birdwell, M. Amani, M. Dubey, M. S. Dresselhaus, T. Palacios and J. Kong, *ACS Nano*, 2014, **8**, 6491–6499.
9 M. Eizenberg and J. M. Blakely, *Surf. Sci.*, 1979, **82**, 228–236.
10 C. Barth, *J. Phys. Chem. C*, 2017, **122**, 522–529.
11 T. Yang, W. Chen, H. Zhang, L. Ma and Y.-Q. Fu, *Mater. Sci. Eng., A*, 2022, **835**, 142662.
12 J. Xiang, L. Ma, Y. Sun, S. Dong, Q. Xu, X. He, Y. Zhou and C. Hai, *Langmuir*, 2024, **40**, 23853–23863.
13 X. Zhang, Y. Xu, M. Wang, E. Liu, N. Zhao, C. Shi, D. Lin, F. Zhu and C. He, *Nat. Commun.*, 2020, **11**, 2775.
14 Y. Chen, X. Zhang, E. Liu, C. He, C. Shi, J. Li, P. Nash and N. Zhao, *Sci. Rep.*, 2016, **6**, 19363.

15 M. Cao, D.-B. Xiong, Z. Tan, G. Ji, B. Amin-Ahmadi, Q. Guo, G. Fan, C. Guo, Z. Li and D. Zhang, *Carbon*, 2017, **117**, 65–74.
16 M. Wang, L.-D. Wang, J. Sheng, Z.-Y. Yang, Z.-D. Shi, Y.-P. Zhu, J. Li and W.-D. Fei, *J. Alloys Compd.*, 2019, **798**, 403–413.
17 Z. Li, P. Wu, C. Wang, X. Fan, W. Zhang, X. Zhai, C. Zeng, Z. Li, J. Yang and J. Hou, *ACS Nano*, 2011, **5**, 3385–3390.
18 X. Gan, H. Zhou, B. Zhu, X. Yu, Y. Jia, B. Sun, M. Zhang, X. Huang, J. Liu and T. Luo, *Carbon*, 2012, **50**, 306–310.
19 J.-H. Choi, Z. Li, P. Cui, X. Fan, H. Zhang, C. Zeng and Z. Zhang, *Sci. Rep.*, 2013, **3**, 1925.
20 Z. Gao, T. Zuo, M. Wang, L. Zhang, B. Da, Y. Ru, J. Xue, Y. Wu, L. Han and L. Xiao, *Carbon*, 2022, **186**, 303–312.
21 K. M. Yang, Q. Li, Q. Zhang, G. S. Liu, J. J. Wang, Y. F. Yang, C. X. Guo, J. M. Ni, J. Song, J. Zhang, Y. Liu and T. X. Fan, *Acta Mater.*, 2022, **226**, 117638.
22 Z. Xu and M. J. Buehler, *J. Phys.: Condens. Matter*, 2010, **22**, 485301.
23 M. S. Dresselhaus, A. Jorio, M. Hofmann, G. Dresselhaus and R. Saito, *Nano Lett.*, 2010, **10**, 751–758.
24 S. C. Yoo, D. Lee, S. W. Ryu, B. Kang, H. J. Ryu and S. H. Hong, *Prog. Mater. Sci.*, 2023, **132**, 101034.
25 K. Chu, F. Wang, X.-h. Wang and D.-j. Huang, *Mater. Sci. Eng., A*, 2018, **713**, 269–277.
26 T. Li, Y. Wang, M. Yang, H. Hou and S. Wu, *Mater. Sci. Eng., A*, 2021, **826**, 141983.
27 Y. Ding, Z. Liu, D. Zhou and C. Cai, *Carbon*, 2024, **230**, 119640.
28 N. Nan, J. Li, X. Zhang, D. Zhao, F. Zhu, C. He and N. Zhao, *Carbon*, 2023, **212**, 118153.
29 X. Li, B. Guo, X. Yu, C. Yang, S. Zhou, S. Cui, Z. Zhang and W. Li, *Composites, Part A*, 2024, **179**, 108032.
30 Y. Yang, Y. Liang, G. He and P. Luo, *Mater. Sci. Eng., A*, 2022, **847**, 143349.
31 C.-C. Chan, W.-L. Chung and W.-Y. Woon, *Carbon*, 2018, **135**, 118–124.
32 A. C. Levi and M. Kotrla, *J. Phys.: Condens. Matter*, 1997, **9**, 299–344.
33 K. Yan, H. Peng, Y. Zhou, H. Li and Z. Liu, *Nano Lett.*, 2011, **11**, 1106–1110.
34 Y. Li, Y. Wu, D. Qin, X. Qiu, Z. Wang, Q. Zhou, S. Yu, Q. Li, H. Li, S. Li, C. Yu, Y. Hu, S. Wang, B. Chen, X. Song, J. Qiang, L. Zhou, Y. Li, N. Xu, M. Liu, W. Yin, X. Sun, L. Sun and Z. Liu, *Small*, 2024, **21**, 2405854.